Langmuir

Article

pubs.acs.org/Langmuir

Playing with Peptides: How to Build a Supramolecular Peptide Nanostructure by Exploiting Helix···Helix Macrodipole Interactions

E. Gatto,*[,†] A. Porchetta,[†] M. Scarselli,[‡] M. De Crescenzi,[‡] F. Formaggio,[§] C. Toniolo,[§] and M. Venanzi[†]

[†]Department of Chemical Sciences and Technologies, University of Rome "Tor Vergata", 00133 Rome, Italy

[‡]Department of Physics, University of Rome "Tor Vergata", 00133 Rome, Italy

[§]Institute of Biomolecular Chemistry, CNR, Padova Unit, Department of Chemistry, University of Padova, 35131 Padova, Italy

Supporting Information

ABSTRACT: A novel method to build bicomponent peptide self-assembled monolayers (SAMs) has been developed, by exploiting helix···helix macrodipole interactions. In this work, a peptide-based self-assembled monolayer composed of two helical peptides was immobilized on a gold surface. Specifically, a pyrene-containing octapeptide, devoid of any sulfur atom (A8Pyr), and a hexapeptide, functionalized at the N-terminus with (*S*,*R*) lipoic acid, for binding to gold substrates (SSA4WA) via a Au−S linkage, have been employed. Both peptides investigated attain a helical structure, because they are almost exclusively formed by strongly folding inducer C^{α}-tetrasubstituted α-amino acids. We demonstrate that the two peptides generate a stable supramolecular nanostructure (a densely packed bicomponent peptide monolayer), where A8Pyr is incorporated into the SSA4WA palisade by exploiting helix···helix macrodipole interactions. The presence of both peptides on the gold surface was investigated by spectroscopic and electrochemical techniques, while the morphology of the monolayer was analyzed by ultra high-vacuum scanning tunnelling microscopy. The composition of the bicomponent SAM on the surface was studied by a combination of electrochemical and spectroscopic techniques. In particular, the amount of Au−S linkages from the sulfur-containing peptides was quantified from reductive desorption of the peptide-based SAM, while the amount of A8Pyr was estimated by fluorescence spectroscopy. The antiparallel orientation of the A8Pyr and SSA4WA peptide chains minimizes the interaction energy between the helix dipoles, suggesting that this kind of electrostatic phenomenon is the driving force that stabilizes the bicomponent SAM.

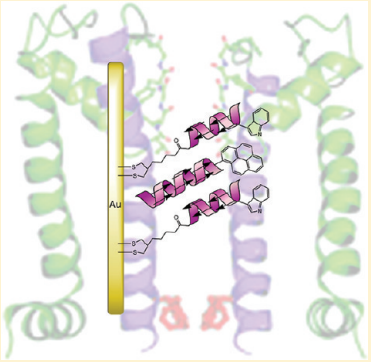

INTRODUCTION

Supramolecular chemistry is certainly one of the most interesting and promising area of chemistry. Although relatively young, it has advanced rapidly over the years and has now reached a high level of sophistication and maturity.[1] Many supramolecular species have been synthesized with the purpose of obtaining materials with interesting and useful properties,[2] or just for constructing architectures of esthetical interest.[3] Different molecules can be assembled together by intermolecular interactions to give supramolecular entities, in analogy to biological systems[4] whereby buildings blocks self-associate in a particular pattern to form a higher order organized complex. The key advantage of using self-assembly[5] is that it capitalizes on the formation of noncovalent and reversible interactions, including electrostatic, hydrophobic, van der Waals and metal···ligand interactions, hydrogen bonds, and aromatic π-stacking. Collectively, if in sufficient number, these weak interactions can yield highly stable assemblies.

This type of approach, universally denoted as "bottom-up" approach,[1−6] is thought to offer substantial advantages compared to the conventional "top-down" approach, that is, lithographic miniaturization techniques for the construction of structures with features between 1 and 50 nm.[7]

The capability to generate smaller structures with respect to classical lithographic methods is of fundamental importance in modern science and technology, for instance, in microelectronics, where smaller means more components in the same space, faster and less expensive operations, lower power consuming, and so forth. In 1983, Nuzzo and Allara[8] first reported on the formation of self-assembled monolayers (SAMs) by the spontaneous adsorption of dialkyl disulfides on gold by covalent Au−S linkage. Since then, many reports have appeared in the literature about SAMs having different thicknesses (chain lengths) and exterior surface functionalities.[9] In one of the first contributions to the field, Samulski and coworkers[10] showed that also α-helical oligopeptides containing a disulfide moiety are promising self-assembly materials. In fact, in nature, the three-dimensional structure of proteins is driven by a number of noncovalent interactions, among them the aggregation of helical segments into a more specific spatial conformation.[11]

In general, the ability to form tightly packed surfaces depends on the length of the peptides and their 3D-structure. Usually, short peptides populate several conformations, they are very flexible and rapidly interconverting between the different conformers. Mainly for this reason, they form loosely packed

Received: November 10, 2011
Revised: December 27, 2011
Published: January 3, 2012

   dx.doi.org/10.1021/la204423d | *Langmuir* 2012, 28, 2817−2826

films that show a large degree of inhomogeneity and have up to 15% vacant gold sites.[12] By contrast, longer helical peptides form well ordered and densely packed films. The capability to form a tightly packed SAM depends not only on the length of the peptide primary structure, but also on the type of secondary structure attained by the peptide chains and on the presence of aromatic groups in the molecules. We have recently demonstrated that also very short peptides (just six residues long) feature very good self-assembly properties if they are folded in a helical conformation, and that these properties can be remarkably improved if they are functionalized with properly arranged aromatic chromophores.[13−15] Short peptides can be constrained to populate helical conformations by using C^{α}-tetrasubstituted α-amino acids, which impose a marked restriction on the available ϕ, ψ space, thus conferring stability to those 3D-structures and, hence, making peptides good candidates as building blocks for the construction of self-assembled nanostructures.

It is well established that helical peptides have a large macrodipole moment (3.5 D per residue)[16] which is oriented parallel to the molecular axis (directed from the N- to the C-terminus). The impact of the resulting electric field on protein structure and function has been also emphasized. The direction of the molecular dipole moment has been demonstrated to be an important variable because it has a significant impact on the direction of the electron transfer processes and on the SAM package as well. Miura et al.[17] reported significant surface potentials for oriented polypeptide SAMs. Moreover, several papers demonstrated that electron transfer (ET) processes occur more rapidly from the C- to N-terminus direction than along the opposite direction, both in solution[18] and on surface.[14,19,20] Kimura and co-workers[20] demonstrated that the immobilization of a bicomponent SAM composed of two helical peptides in which the gold binding (*S*,*R*) lipoic group was linked either at the C- or at the N-terminus, respectively, can generate a more packed monolayer as compared to a SAM in which the helical peptide macrodipoles are aligned in a parallel way. This effect was ascribed to the attractive interchain interactions taking place between opposing dipoles in the bicomponent SAM. Also Kraatz and co-workers[21] demonstrated that, even if peptide SAMs are dynamical systems, in the antiparallel dipole arrangement, peptides experience a more restricted motion due to stronger intermolecular interactions. Recently, the assembly of molecular architectures on the basis of molecular dipoles has been proposed as a promising tool for construction of nanomaterials and nanodevices.[22]

In this contribution, we demonstrate that it is possible to immobilize a photoactive peptide without a sulfur group on a gold surface, just by exploiting noncovalent interactions. We recently designed a short 3_{10}-helical peptide[13,14] based on the strongly folding inducer C^{α}-tetrasubstituted α-aminoisobutyric acid (Aib) residue,[23,24] containing an L-tryptophan (Trp) unit and functionalized at the N-terminus by an (*S*,*R*) lipoyl (Lipo) anchoring group (SSA4WA, Figure 1), which was able to form a tightly packed SAM on a Au surface and to generate photocurrent under illumination.[14] Here, in combination with SSA4WA, we exploited a longer, conformationally constrained, 3_{10}-helical peptide, based on the C^{α}-tetrasubstituted Aib, Api (4-aminopiperidine-4-carboxylic acid) and L-(αMe)Nva (C^{α}-methyl norvaline)[24] residues, bearing a 1-pyrenyl (Pyr) unit in the proximity of the N-terminus and devoid of any Lipo or other S-containing groups (A8Pyr, Figure 1). In particular, we show that, by taking advantage of helix···helix macrodipole

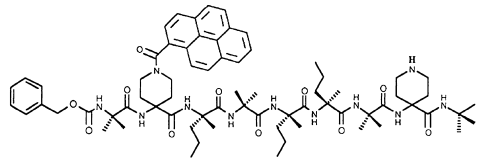

A8Pyr: *Z-Aib-Api(Pyr)-L-(aMe)Nva-Aib-L-(aMe)Nva-L-(aMe)Nva-Aib-Api-(Boc)-NHtBu*

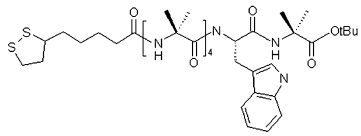

SSA4WA: *Lipo-Aib$_4$-L-Trp-Aib-OtBu*

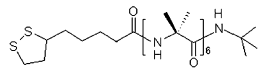

SSA6: *Lipo-Aib$_6$-NHtBu*

Figure 1. Chemical formulas and acronyms for the peptides investigated in this work (Z, benzyloxycarbonyl; Boc, *tert*-butyloxycarbonyl; *t*Bu, *tert*-butyl).

interactions, immobilization of even an S-lacking peptide and construction of a stable supramolecular system are feasible. Indeed, we prepared a mixed SAM formed by SSA4WA, covalently linked to gold, and A8Pyr embedded into the SSA4WA chains, working in peptide aggregative conditions, by adding 25% of water to the ethanolic incubation solution. The inclusion of the pyrenyl containing peptide in the bicomponent SAM was demonstrated by fluorescence and electrochemical experiments, while the film morphology was investigated by ultrahigh vacuum (UHV) scanning tunnelling microscopy (STM). Furthermore, a new method to determine the composition of bicomponent SAMs on a surface was developed by combining electrochemical and spectroscopic techniques. The amount of Au−S linkages was quantified by the reductive desorption of the peptide-based SAM, while that of the Pyr functionalized peptide was estimated by fluorescence spectroscopy. We believe that dipolar noncovalent interactions can be usefully exploited in the construction of supramolecular architectures, thus developing the so-called "molecular dipole engineering" approach.[22]

EXPERIMENTAL SECTION

Materials. The synthesis and the chemical and conformational characterizations of the peptides SSA4WA, SSA6, and A8Pyr were reported elsewhere.[13−15] Spectrograde solvents (Carlo Erba) were exclusively used. Water was distilled and passed through a Milli-Q purification system. Other chemicals, triethanolamine (TEOA) (Fluka), potassium chloride (Carlo Erba), sodium sulfate (Carlo Erba), potassium ferricyanide (Aldrich), and potassium hydroxide (Aldrich) were all of reagent grade quality and used without further purification.

Gold Substrates. Ultraflat gold substrates were used to perform STM measurements. They were prepared by thermal evaporation of gold on mica sheets (template stripped method).[25] Gold evaporation was performed at 3×10^{6} mbar, $T = 573$ K, and at 0.1 nm/s deposition rate until a 200 nm thick film was formed. Mica/gold substrates were glued onto a Si(100) wafer by an epoxydic paste and then annealed for 1 h at 423 K. This procedure makes it possible to keep the mica/gold/Si wafer safe for several months. In due time, the mica was carefully removed after immersion in tetrahydrofuran, and the gold substrate was repeatedly rinsed with ethanol and dried by flushing the surface with ultrapure nitrogen. The (111) character of the gold surface is reported in the Supporting Information. Gold foil electrodes of 0.05

mm thickness were bought from Sigma-Aldrich and used for electrochemical measurements. Transparent glass coated with a 5 nm thick Au layer was a Nanocs product and used for fluorescence measurements.

Preparation of Self-Assembled Peptide Thin Films. Gold electrodes were etched for 15 min in a freshly prepared piranha solution (2:1 sulfuric acid/H_2O_2, *v/v*) and then rinsed with bidistilled water and ethanol before immersion in the peptide solution for the SAM deposition. SAM-coated electrodes were prepared by dipping the cleaned gold electrode into an 1 mM ethanol solution of the peptide in a N_2 atmosphere. After 18 h, the electrode was repeatedly (five times) rinsed with ethanol to remove physically adsorbed peptides from the SAM and dried for 3 min under a gentle argon flow. The bicomponent peptide SAM was prepared by mixing two 0.5 mM ethanol/water 3:1 v/v solutions of the two peptides. Deposition time and rinsing procedures were the same as those used for the preparation of single-component SAMs. Water was added to favor the aggregation of A8Pyr/SSA4WA peptides, already in solution. In this experimental conditions, fluorescence measurements show Förster energy transfer processes from the excited tryptophan moiety to the pyrene chromophore, confirming the two peptides to be close to each other.

Methods. *Electrochemistry.* Cyclic voltammograms (CVs) were obtained by using a PG 310 potentiostat (Heka Elektronik). CV experiments were carried out at room temperature, adopting a standard three-electrode configuration with a SAM-coated gold electrode as the working electrode, a platinum wire as the auxiliary electrode, and Ag/AgCl as the reference electrode. Blocking experiments were carried out with a 0.5 mM $K_3Fe(CN)_6$ solution in 1 M KCl at a sweep rate of 50 $mV{\cdot}s^{-1}$. Photocurrent measurements were carried out at room temperature using the three-electrode setup described above, by using Na_2SO_4 (0.1 M) as supporting electrolyte and TEOA (50 mM) as the electron donor in solution. In this experiment, the SAM-modified electrode was irradiated with a Xe lamp (150 W) equipped with a monochromator, and the generated photocurrent was detected by the voltammetric analyzer described above. The incident photon-to-current efficiency (IPCE) has been determined by using the following equation:[26]

$$\text{IPCE}\ (\%) = \frac{100 \times i(\text{A/cm}^2) \times 1240}{I(\text{W/cm}^2) \times \lambda(\text{nm})}$$

where i is the measured photocurrent, I is the incident light power density, and λ is the incident wavelength (340 nm). The intensity of the incident light was evaluated by azobenzene actinometry.[27]

Reductive desorption measurements were carried out by bubbling argon in the 0.5 M KOH electrolyte solution for at least 30 min prior to the desorption measurement.

Steady-State Fluorescence. Steady-state fluorescence experiments were carried out on a Fluoromax spectrofluorimeter (Jobin-Yvon) operating in the single-photon counting mode. For the fluorescence measurements, the peptide SAMs were immobilized on a transparent glass coated with a 5 nm thick Au layer. The glass was mounted on a solid sample holder and the signal detected at 30° for minimizing scattered light contamination.

Scanning Tunneling Microscopy Measurements. Scanning tunneling microscopy imaging was performed at room temperature using an Omicron-STM system. Electrochemically etched tungsten tips were employed for the experiments. STM calibration was done by comparing images of molecular adsorbates with atomically resolved ones of highly oriented pyrolitic graphite. All images were unfiltered apart from rigid plane subtraction.

RESULTS AND DISCUSSION

Cyclic voltammetry (CV) experiments showed that, after 24 h incubation of a gold electrode into a 1:1 (mol/mol) SSA4WA/A8Pyr peptide solution, a SAM on the gold electrode is formed, that inhibits almost completely the $K_3[Fe(CN)_6]$ electrolyte discharge (Figure 2).[28] We already demonstrated that a six-residue 3_{10}-helical peptide was able to form a very densely

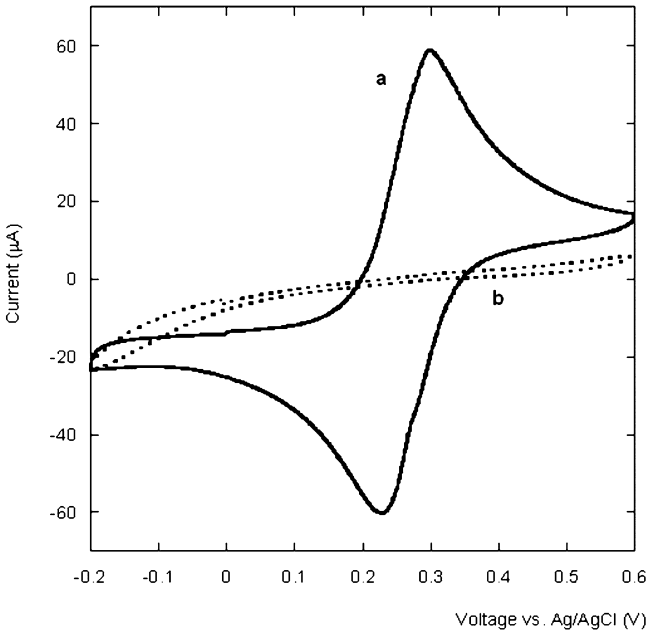

Figure 2. Cyclic voltammetry experiments in a 0.50 mM $K_3[Fe(CN)_6]$ aqueous solution: (a) bare gold electrode; (b) gold electrode modified by the mixed peptide SAM. Sweep rate: 50 mV/s.

packed SAM, the surface density of which was very close to what expected assuming a vertical orientation and a close hexagonal packing of helical peptides.[14] Indeed, the cross-sectional area of a 3_{10}-helix is 0.69 nm^2 (9.4 Å diameter).[29] Therefore, assuming a tilt angle with respect to the surface normal of 0°, a 3_{10}-helical peptide monolayer is expected to exhibit a surface density of 21.7×10^{-11} mol/cm^2.[29] However, it is generally found that peptide SAMs are never perpendicularly oriented and their axis has a tilt angle of 30−60° with respect to the surface normal.[29,30] As a consequence, the surface density value is reduced to $18.8-10.9 \times 10^{-11}$ mol/cm^2. In conclusion, to know the real surface density, the theoretical value should be multiplied by the cosine of the tilt angle that the peptide helical axis forms with respect to the normal to the gold surface.[29]

To assess the presence of the A8Pyr peptide in the monolayer, we performed fluorescence and photocurrent generation experiments on the A8Pyr/SSA4WA mixed SAM in the Pyr spectral region. Pyr is a spatially sensitive fluorescent probe, which forms excited-state dimers (excimers) upon a close encounter with another Pyr-containing molecule (Figure 3a).[31,32] Therefore, the observation of an excimer emission indicates, in a bicomponent SAM, the formation of raft domains, that is, segregated single-component regions. Formation of Pyr···Pyr excimers has been already observed by us in a single component peptide SAM functionalized with a lipoic acid and a Pyr antenna group.[15] The fluorescence spectrum of the A8Pyr/SSA4WA SAM exhibits the typical emission band of the Pyr monomer fluorophore (Figure 3b), with a maximum at 397 nm, which confirms the A8Pyr inclusion into the SAM. Interestingly, the fluorescence spectrum shows only a small broadening of the Pyr emission band, excluding short-range pyrene···pyrene interactions in the peptide film. This finding also suggests that A8Pyr is intercalated within the SSA4WA palisade quite homogeneously, as only in that case each pyrene chromophore is located quite distant from the others.

dx.doi.org/10.1021/la204423d | *Langmuir* 2012, 28, 2817−2826

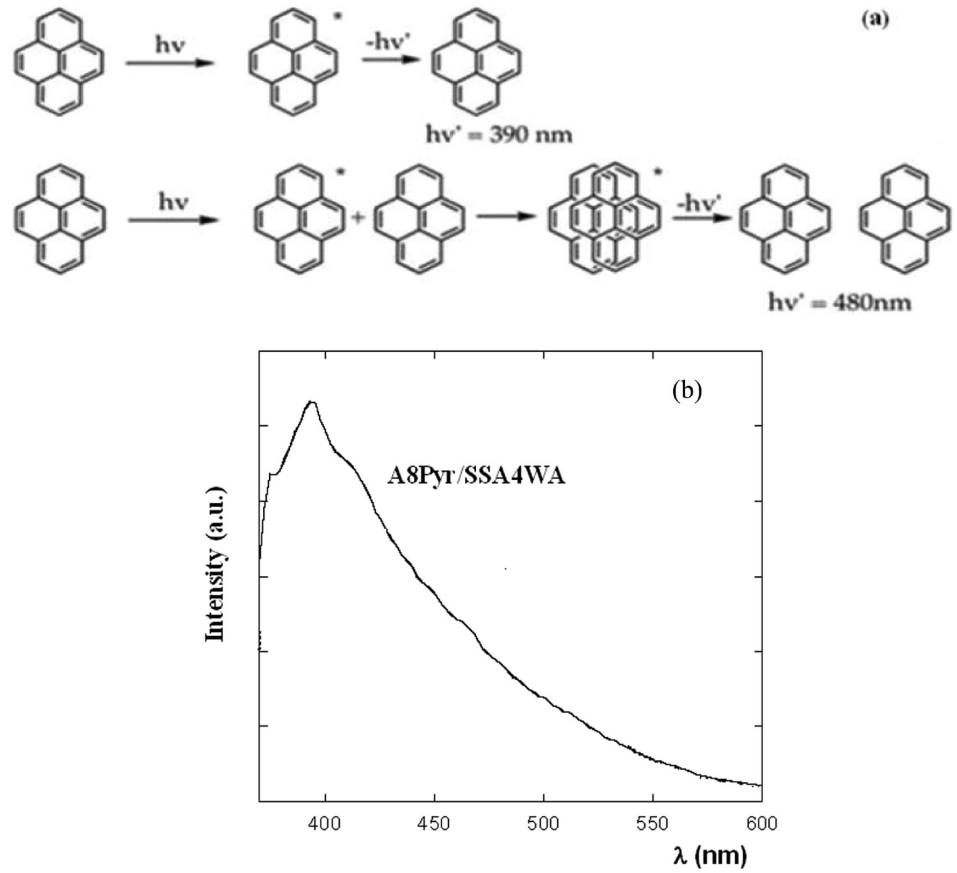

Figure 3. (a) Schematic representation of the pyrene monomer and excimers, and their corresponding fluorescence wavelengths. (b) Fluorescence experiment in the pyrene emission region. Spectrum of the gold (5 nm)/glass slide/mixed peptide SAM. Excitation wavelength: λ = 340 nm.

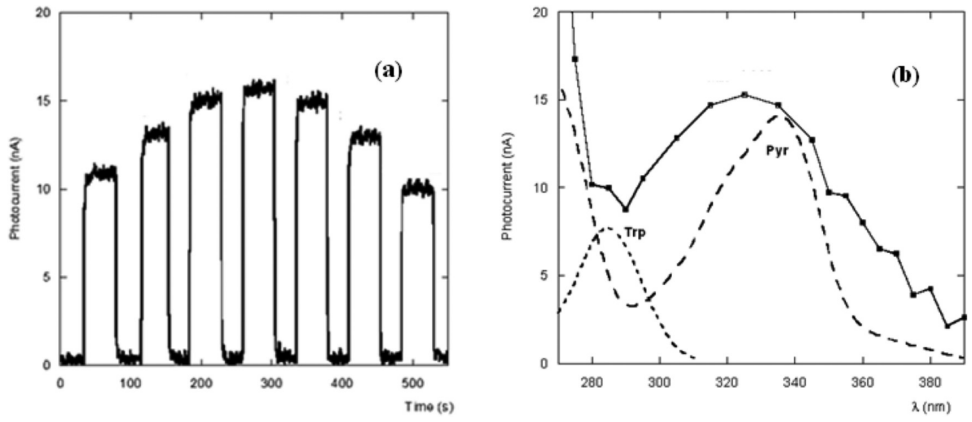

Figure 4. (a) Time course of the photocurrent of the bicomponent SAM in an aqueous TEOA solution at 0 V vs Ag/AgCl upon photoirradiation at different wavelengths (every 10 nm from 295 to 355 nm) at room temperature. (b) Photocurrent action spectrum of the gold electrode modified by deposition of the bicomponent A8Pyr/SSA4WA SAM in ethanol (—•—), as compared to the excitation (15 nm slit width) spectra of the isolated Pyr (– – –) and Trp (- - -) chromophores.

Photocurrent generation experiments also confirmed the presence of the A8Pyr peptide embedded into the SSA4WA matrix. These experiments are recently arousing remarkable interest because of their potential in understanding natural photosystems and their applications in molecular electronics. In the past few years, Kimura and co-workers and our groups[13−15,20,33−35] reported on several α- and 3_{10}-helical peptide SAMs on gold surfaces functionalized with light-harvesting chromophores to mimic natural photosystems. They found that upon illumination in the chromophore absorption region high anodic or cathodic currents are generated (antenna effect), depending on the redox active electrolyte in solution. Specifically, in the presence of an electron donor in solution, an electron transfer (ET) process from the photoexcited chromophore to the gold surface was observed. On the other hand, in the presence of an electron acceptor in solution, the direction of the current was reversed and ET from the gold surface to the chromophore occurred. These results were explained on the basis of photoinduced ET reactions mediated by the peptide matrix.

dx.doi.org/10.1021/la204423d | *Langmuir* 2012, 28, 2817−2826

We performed photocurrent generation measurements on a gold electrode modified by deposition of a A8Pyr/SSA4WA mixed SAM in an aqueous solution of triethanolamine (TEOA), a well-known electron donor. Upon illumination in the Pyr absorption region, an intense anodic current was measured. The current generated upon photoirradiation of the peptide SAM at different wavelengths (15 nm bandwidth) in the presence of TEOA is shown in Figure 4a, where repeated on−off cycles of photoexcitation, each one 30 s long, are reported. Remarkably, the action spectrum, that is, the photocurrent response versus the excitation wavelength, of the mixed SAM almost perfectly overlaps the excitation spectra of Pyr and Trp measured in ethanol solution using the same slit opening conditions (15 nm) (Figure 4b). It is worth noting that both the bare gold electrode and the electrode modified by a peptide SAM not functionalized with a Pyr antenna group (SSA6), also synthesized for control experiments, generated just a very weak photocurrent signal under the same experimental conditions (Figure 5). Interestingly, the incident

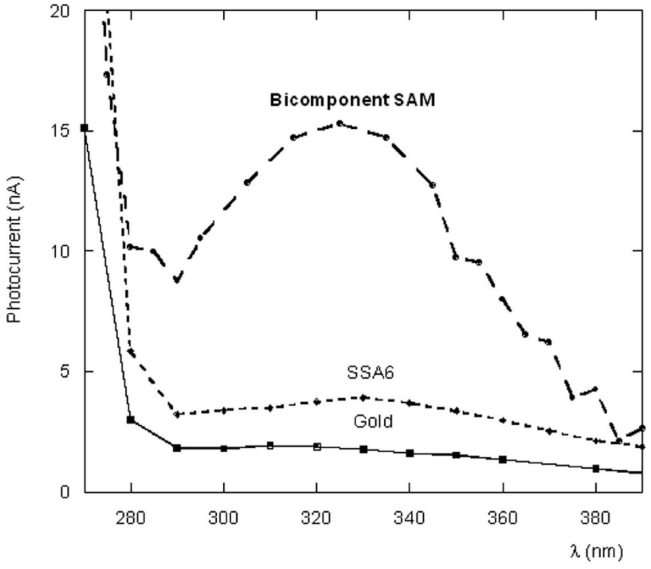

Figure 5. Photocurrent action spectrum of the gold electrode modified by deposition of the bicomponent A8Pyr/SSA4WA SAM in ethanol (●), as compared to the photocurrent action spectra, obtained under the same experimental conditions, of the bare gold electrode (■), and of the pyrene devoid peptide SSA6 SAM (◆).

photon to current efficiency (IPCE%) for the bicomponent A8Pyr/SSA4WA SAM at λ = 340 nm (Pyr absorption maximum) was found to be equal to 0.02%, while the SSA6 modified electrode showed an IPCE% value at the same excitation wavelength of 0.002%.

Recently, Kraatz and co-workers[36] showed that significant photocurrent signals are generated even in the absence of peptide films or antenna probes. They explained these results by ascribing most of the measured photocurrent to a simple photothermal effect, that is, a potential drop caused by heating of the diffusion layer at the electrode interface upon illumination. Indeed, in their experiments, they were able to demonstrate that a photocurrent signal may be obtained by irradiating a bare gold electrode with a laser. They also claimed that the enhanced photocurrent signal measured in the presence of a chromophore-containing peptide could be correlated to the increase in temperature due to UV-absorption of the chromophore. In our case, the photothermal effect is most likely responsible for the very weak signal measured in the case of the bare gold electrode and the peptide film without Pyr (SSA6). In the case of the A8Pyr/SSA4WA mixed SAM, instead, a very high photocurrent signal, which corresponds to the Pyr absorption spectrum, was obtained, although in our experiment excitation in the UV region was achieved by a much less powerful Xe lamp. To clarify the origin of this signal, we performed photocurrent generation measurements at the potential at which SSA6 has a zero current response (−0.15 V). This potential value corresponds to the maximum entropy of formation of the double layer and where the photothermal effect is zero.[36] Under these conditions, a high photocurrent signal was also obtained, which indicates that the photothermal effect can be safely considered only as a minor contribution to the whole photocurrent. In any case, irrespectively of the photocurrent signal interpretation, these results demonstrate the presence of the Pyr-containing peptide into the SSA4WA matrix. From these experiments, we can conclude that the A8Pyr peptide is embedded inside the SSA4WA layer and that each Pyr chromophore is quite apart from the others. However, at this point, we do not have any decisive information about the A8Pyr orientation in the SSA4WA film.

Nevertheless, photocurrent generation measurements provide some hints about the orientation of the Pyr-containing peptide, suggesting it to be close to the electrolyte solution. In this connection, Kimura and co-workers[33] demonstrated that the capability of a peptide to generate current depends on the position of the redox active group along the peptide sequence. In their study of two different peptides carrying a disulfide group at the N-terminus and a naphthyl group at the N- or C-terminus (denoted respectively as SSNA2B and SSA2NB), they discovered that, when the naphthyl group is covalently bound at the peptide N-terminus (SSNA2B), any photocurrent signal is seen, while when the naphthyl group is bound at the peptide C-terminus (SSA2NB), a photocurrent signal is easily observed. They explained these results by ascribing the photocurrent signal loss to the inhibition of TEOA diffusion to the naphthyl chromophore. Indeed, ET from TEOA to the naphthyl group needs the electrolyte to be close to the peptide chromophore. In the case of the SSNA2B peptide SAM, the naphthyl is far away from the aqueous solution and the diffusion of the redox active electrolyte is strongly suppressed. Our results demonstrate that the Pyr moiety is able to give rise to a net anodic photocurrent signal, which strongly suggests it to be in contact with the TEOA solution.

To investigate the SAM morphology after the introduction of the A8Pyr peptide into the SSA4WA palisade, we performed UHV STM experiments. Previous experiments carried out on the SSA4WA SAM showed formation of a homogeneous peptide monolayer, chemisorbed on the gold substrate through Au−S linkages.[13] However, in that case, we did not succeed in observing a single helical peptide molecule. It should be noted that identification of a single helical peptide molecule in a monocomponent helical peptide SAM has never been reported and it is not observable even at high resolution STM. Plausible reasons are that all peptides have the same height and intermolecular lateral electron hopping occurs, which make the molecular imaging ambiguous.[37]

Kimura and co-workers[38,39] succeeded in the observation of a single helical peptide by STM microscopy, in the course of a study of a bicomponent SAM formed by incorporating a helical peptide into an alkanethiol monolayer. In this case, a single

dx.doi.org/10.1021/la204423d | Langmuir 2012, 28, 2817−2826

helical peptide molecule was imaged, because it was protruding from the surrounding alkanethiol SAM.

Figure 6 shows the UHV STM image of the bicomponent SAM formed by A8Pyr and SSA4WA. This image shows the

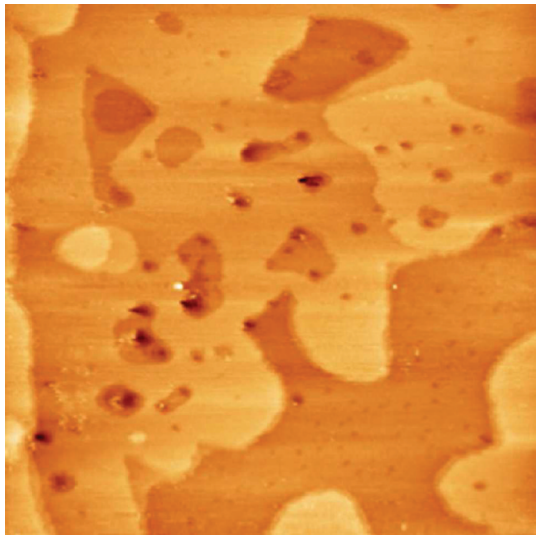

Figure 6. Constant current STM image (250 nm × 250 nm) of the A8Pyr/SSA4WA mixed peptide SAM. Image recorded at a sample bias of 2.5 V and a tunnelling set current of 90 pA.

typical features of the peptide SAMs: film domain boundaries, vacancy islands which are usually observed for monolayers prepared at room temperature, Au substrate terraces separated by single atom steps, and the $(\sqrt{3} \times \sqrt{3})$ R30° hexagonal surface structure.[40] Images of the clean Au substrate may be found in the Supporting Information.

Holes of 0.2−0.3 nm depth and 2−6 nm width are considered as good evidence for the formation of a homogeneous peptide monolayer, chemisorbed on the gold substrate through Au−S linkage,[38] as they are formed during the S−Au binding process, due to the Au etching. These features have often been found in SAMs formed by alkanethiols,[41] and have been also observed in STM experiments on peptide SAMs.[37] Furthermore, in agreement with fluorescence measurements, the monolayer appears to be rather homogeneous with no apparent raft domains, that is, segregated single-component regions. Interestingly, the bicomponent SAM does not show any stripelike morphology on the surface, typical of surface lying molecules,[13,42] which suggests that both types of peptides are vertically oriented on the gold surface.

To further characterize the bicomponent SAM, STM measurements changing the applied bias were carefully performed. STM images of the A8Pyr/SSA4WA mixed SAM, acquired with a stepwise increase of bias voltage from 1.0 to 3.5 V and then decreased back to 2.0 V, are shown in Figure 7. Many bright spots are clearly observed at highly positive bias voltages (Figure 7c). The size of these spots is always the same from place to place in the flat terraces. In the high resolution images, it is possible to determine the diameter of each dot. A geometrical analysis of the dot diameters was therefore performed in Figure 8. It shows that most of the bright spots

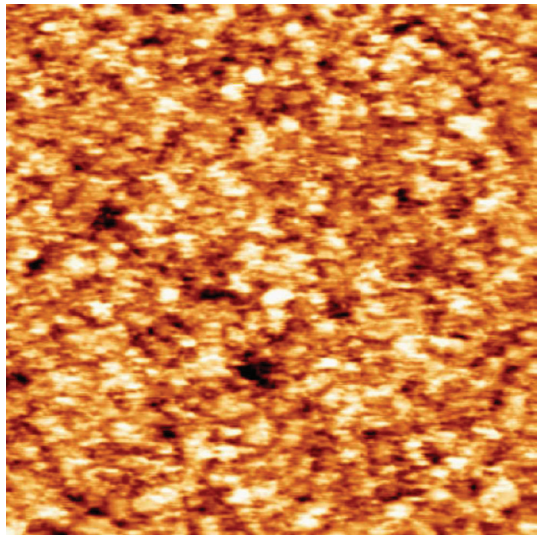

Figure 8. Constant current STM image of the bicomponent SAM. Many bright spots were observed. The diameter of each spot is 1 nm. This image was recorded with a sample bias of 3.8 V and a tunneling current set of 60 pA.

has a diameter of 1 nm (Supporting Information). Average height differences of the spots from the surrounding matrix in the STM images were approximately 2.0 ± 0.5 Å. The bright spots are absent in Figure 7d obtained at 2.0 V applied voltage. This result suggests the complete reversibility of the process and highlights the good stability of the film after repeated scans. These remarkable properties have been also confirmed following acquisition of images on more extended sample areas at different applied voltages (Supporting Information).

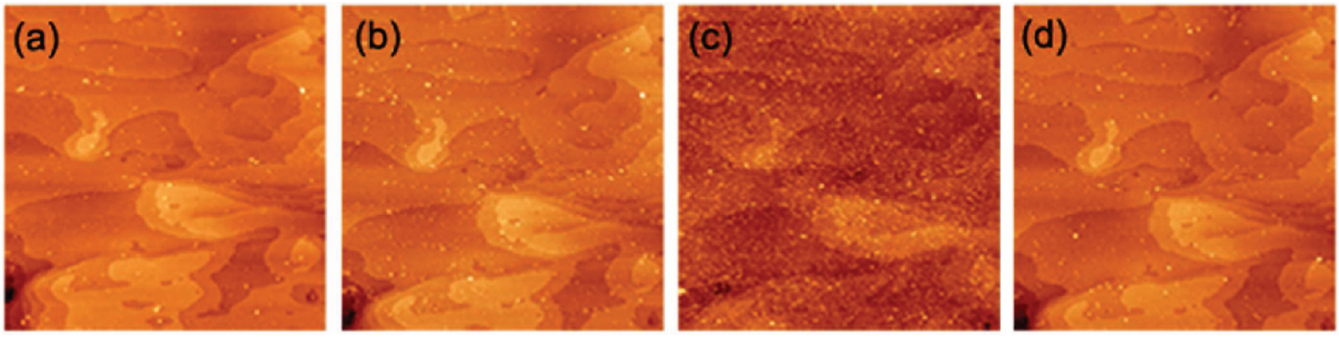

Figure 7. STM images (350 nm × 350 nm) of the bicomponent SAM obtained with stepwise increase of bias voltage from (a) 2.0 V, (b) 2.5 V, (c) 3.5 V, and back to (d) 2.0 V.

dx.doi.org/10.1021/la204423d | *Langmuir* 2012, 28, 2817−2826

In the literature, dots observed on a bicomponent SAM formed by incorporation of helical peptides into an alkanethiol monolayer were interpreted as a single helical peptide protruding from the surrounding dodecanethiol SAM.[38,39] Interestingly, the identification of such dots in a similar alkanethiol/peptide SAM was taken as evidence of a conformational transition from the shorter α-helix to the more elongated 3_{10}-helix conformation by changing the polarity of the applied bias as a result of the interaction of the electric field with the helix dipole moment.[39] In our case, the diameter of the dots found in the STM measurements well agrees with that of a 3_{10}-helix (ca. 1 nm), letting us to consider each dot as representing a single helical peptide protruding from the surrounding peptide SAM. In any case, in analyzing the STM images, we cannot neglect the different electron density of the A8Pyr and SSA4WA peptides. The A8Pyr peptide, because of the presence of the Pyr moiety, has a higher electron density as compared to that of the SSA4WA peptide. This property can give rise to a brighter image, because of the known high conduction through Pyr-containing molecules.[43] Therefore, the observed contrast in our STM images can be attributed to both the different length of the peptide backbones[38,39,44] and to the influence of the electron density of the chromophoric head groups.[43] However, since all our conclusions assign the bright dots to the A8Pyr peptides, the considerations on the SAM homogeneity and peptides surface orientation hold true. Specifically, the A8Pyr/SSA4WA mixed SAM represents a combination of an hexapeptide (SSA4WA), bound to gold through the N-terminal Lipo group, and an octapeptide (A8Pyr) embedded into the SSA4WA palisade, most likely organized in an antiparallel arrangement. Moreover, photocurrent generation experiments indicate that the Pyr moiety is close to the electrolyte solution. As a result, it is plausible to assume that A8Pyr and SSA4WA are preferentially oriented in an antiparallel arrangement with the negatively charged C-terminus of the A8Pyr dipole lying close to the gold surface (Figure 9). To get further information

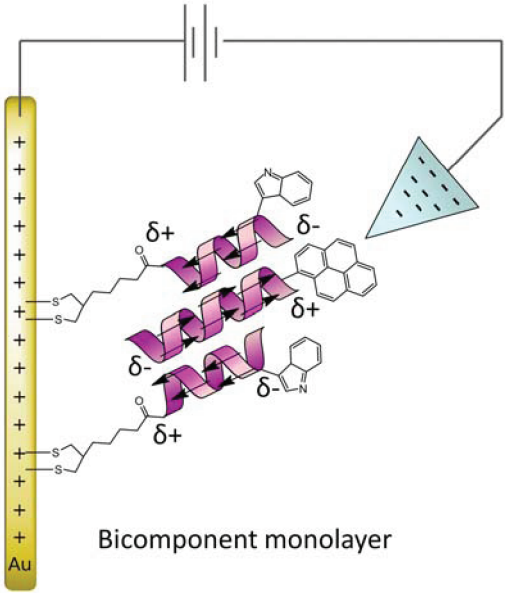

Figure 9. Schematic representation of the bicomponent SAM during STM measurements. The SSA4WA peptide is immobilized onto a gold surface by the N-terminal Lipo group, while the A8Pyr is embedded into the SSA4WA palisade in an antiparallel orientation.

on the A8Pyr orientation in the peptide SAM, we have performed scanning tunneling spectroscopy (STS) measurements. It is well-known that $I-V$ curves of helical peptide SAMs are not symmetric, because of the helical dipole moment which favors the ET reaction occurring in the same direction as that of the electric field.[39] The results of our STS spectroscopy measurements, obtained by statistically averaging the $I-V$ signals, taken at selected points of 50 × 50 nm^2 areas of the surface modified by the peptide deposition, are shown in Figure

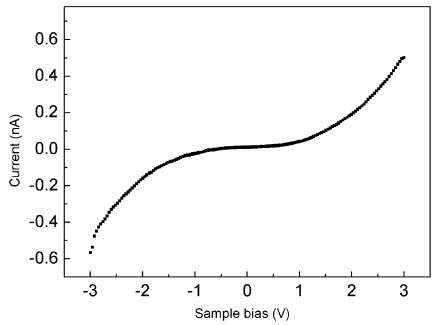

Figure 10. Current−voltage ($I-V$) curve of the bicomponent SAM. The line was obtained by statistically averaging the $I-V$ signals, taken at selected points of 50 × 50 nm^2 areas of the surface after peptide deposition.

10. Interestingly, the $I-V$ curve is highly symmetric, which suggests that there is not a preferred direction for ET. Again, this result supports the view of an antiparallel orientation of the two peptide components, which is also favored by electrostatic considerations. Indeed, the interaction potential between two electric dipoles is given by

$$V_{12} = \frac{\mu_1\mu_2}{R_{12}}(\cos\phi - 3\cos\vartheta_1\cos\vartheta_2)$$

where R_{12} is the dipoles distance, ϕ is the angle between the dipoles, and θ_1 and θ_2 are the angles formed by these dipoles with the line connecting them. As a consequence, two interacting helices will be preferentially aligned in an antiparallel way.

Our statistical analysis, performed in Figure 8, indicates that the dot average height is about 2.5 ± 0.5 Å and that their surface coverage amounts to 33.2%. These findings suggest that the surface stoichiometry is A8Pyr/SSA4WA 1:2 (Supporting Information). To confirm this conclusion, we decided to develop a new method to determine the surface composition of the bicomponent SAM by using a combination of electrochemical and spectroscopic techniques: the amount of Au−S linkages was quantified from the reductive desorption of the peptide-based SAM,[45−47] while the amount of the Pyr-functionalized peptide was estimated from fluorescence spectroscopy.[48]

The first approach is based on the voltammetric measurement of the charge passed for the two-electron reductive desorption of the gold-bound thiolate layer in an alkaline solution:

$$\mathrm{Au(s)} - \mathrm{S}_\lambda\mathrm{R} + \lambda\mathrm{e}^- \rightarrow \mathrm{Au(s)} + \mathrm{R(S^-)}_\lambda$$

In this equation, λ represents the degree of charge transferred between the sulfur atom and the surface (for lipoic acid λ = 2, while for alkanethiols λ = 1).

dx.doi.org/10.1021/la204423d | Langmuir 2012, 28, 2817−2826

The surface coverage due to the gold-bound peptide was estimated from the charge corresponding to the reductive desorption of the lipoic acid from the gold surface.[49,50] Desorption experiments were performed in a 0.5 M KOH aqueous solution. A typical CV curve obtained from this experiment is shown in Figure 11. When the gold electrode

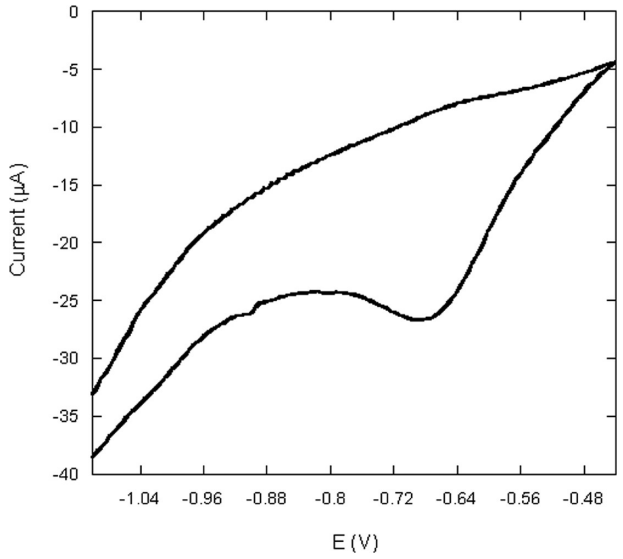

Figure 11. Cyclic voltammetric curve recorded in 0.5 M KOH for the gold electrode modified by the bicomponent peptide SAM. Scan rate: 100 mV/s.

modified with the bicomponent peptide monolayer is immersed in an alkaline solution and the potential is swept to sufficiently negative values, a reduction peak appears, which corresponds to the reductive desorption of the sulfur-containing molecules from the electrode surface.[45−47,49,50] Assuming that each peptide contains two sulfur atom, so that two electrons are involved in the process, the surface coverage of the electrode can be calculated from the peak area (i.e., the charge associated with the reduction process). The surface coverage ascribable to the SSA4WA peptides was found to be $1.0 \pm 0.5 \times 10^{-10}$ mol/cm^2. The surface area of Au gold foil electrodes was determined from the CV of a $K_3[Fe(CN)_6]$ standard solution, following the Randles−Sevcik equation:

$$i_p = 0.4463nFAC(nF\nu D/RT)^{1/2}$$

where i_p is the current maximum, n is the number of electrons transferred in the redox event, A is the electrode area in cm^2, F is the Faraday constant, D is the ferricyanide diffusion coefficient (7.2×10^6 cm^2/s),[51] C is the electrolyte concentration, and ν is the scan rate. We found that the electrode active surface is 1.1 times the geometric surface area of the electrode.

To determine the surface coverage ascribable to the weakly bound A8Pyr peptide, we performed fluorescence spectroscopy measurements. It has been demonstrated that by applying a sufficiently negative potential, gold-bound molecules can be removed from the surface. To ensure the complete removal of the monolayer, we applied for three minutes a −1.5 V voltage (vs Ag/AgCl) in a known amount of ethanol (2 mL). Then, the fluorescence of the electrolytic ethanol solution in the 350−500 nm region was examined by measuring the strong emission characteristic of the Pyr monomer (Figure 12). CV experiments

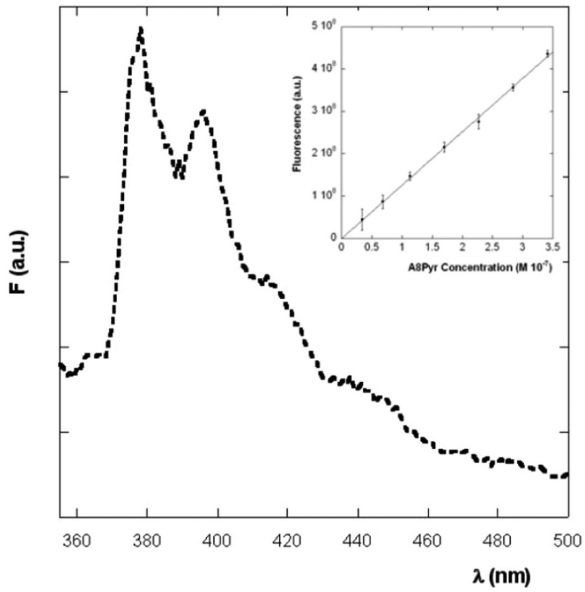

Figure 12. Fluorescence spectrum in the pyrene emission region of the electrolytic ethanol solution used for the SAM removal by electrochemical desorption. Excitation wavelength: λ = 340 nm. Inset: Calibration curve which correlates the A8Pyr fluorescence spectrum intensity (integration performed on the whole spectrum) to its concentration in an ethanol solution. The values are the averages of seven different measurements.

in a 0.50 mM ferricyanide solution, after applying a −1.5 V potential for three minutes, showed a signal comparable to that of the bare gold electrode, which allows us to conclude that the bicomponent SAM is completely removed (Supporting Information). Furthermore, to correlate the fluorescence spectrum to the concentration in ethanol solution, we performed a calibration curve in the expected concentration range (Figure 12, inset). By knowing the volume of ethanol and the immersed area of the SAM covered gold electrode, it was possible to determine the surface coverage due to the A8Pyr peptide, that amounts to $0.6 \pm 0.5 \times 10^{-10}$ mol/cm^2. The total surface coverage was therefore found to be $1.6 \pm 0.5 \times 10^{-10}$ mol/cm^2. This is close to the expected value if we assume a close hexagonal packing for the helical peptides on the surface, with a tilt angle of 40−50° with respect to the surface normal. This finding confirms the good assembly properties of short helical peptides and their almost vertical orientation. Furthermore, the SAM stoichiometry has been found to be SSA4WA/A8Pyr 2:1, in agreement with the surface stoichiometry obtained from our STM statistical analysis.

Since the initial concentration ratio of the deposition solution is 1:1, we would have expected the same surface stoichiometry. But the formation of a SAM is a dynamical process, which requires quite a long time (18 h). Rearrangement and favorite linkage of the thiol-functionalized peptide probably would lead the final composition to 2:1, as a result of the balance between the quite strong Au−S bond (35 kcal/mol) and the weaker electrostatically driven peptide−peptide interactions.

■ CONCLUSIONS

In this work, spectroscopic, electrochemical, and microscopy techniques have been employed for the investigation of a bicomponent SAM composed of two short, conformationally

dx.doi.org/10.1021/la204423d | Langmuir 2012, 28, 2817−2826

constrained peptides, one bearing a lipoic acid group able to bind gold surface and the other having a fluorescent Pyr chromophore but lacking the gold binding group. Electrochemical and fluorescence techniques have been employed to detect the presence of the sulfur-devoid peptides, while STM measurements have been used to characterize the film morphology. Our results indicate that the peptides are oriented in an antiparallel manner by exploiting the favorable interhelical dipole−dipole interactions. It had already been demonstrated that dipolar constituents with specific molecular shapes are useful building blocks for molecular architectures and organization, due to their well-defined 3D-structures and interactions, but, to our knowledge, this is the first example where these weak molecular interactions are used for the construction of a bicomponent peptide-based SAM, where only one component is covalently linked to gold.

Furthermore, we have taken advantage only of short peptides, thus reducing the synthetic costs and favoring the process of electron transfer, because of the short distance between the redox active moiety and the gold surface. In general, it is true that SAMs formed by oligopeptides are unstable, and that these systems are very dynamical,[21] especially during electrochemical experiments. However, we have demonstrated that, by using conformationally constrained amino acids as building blocks, helical peptides can form very densely packed films on a gold surface. The usefulness of suitably functionalized peptides as a sort of LEGO units exploiting dipole···dipole interactions opens important avenues for the design and fabrication of molecular nanostructures based on the "molecular dipole engineering" approach.

■ ASSOCIATED CONTENT

Ⓢ Supporting Information

Circular dichroism spectra of the two peptides in solutions; STM images of the gold surface; STM images of 1 μm·1 μm size at different applied voltages; description of the statistical analysis performed in Figure 8; graph of the geometrical analysis performed in Figure 8 to determine the dots diameter; cyclic voltammograms performed before and after SAM removal. This material is available free of charge via the Internet at http://pubs.acs.org.

■ AUTHOR INFORMATION

Corresponding Author

*Telephone: +390672594469. E-mail: emanuela.gatto@uniroma2.it.

■ ACKNOWLEDGMENTS

The financial support (PRIN 2008, 20088NTBKR) of the Italian Ministry for University and Research (MIUR) is gratefully acknowledged.

■ REFERENCES

(1) (a) Lehn, J. M. *Science* **1985**, *227*, 849−856. (b) Lehn, J. M. *Angew. Chem., Int. Ed. Engl.* **1988**, *27*, 89−112. (c) Lehn, J. M. *Science* **1993**, *260*, 1762−1763. (d) Philip, D.; Stoddart, J. F. *Angew. Chem., Int. Ed. Engl.* **1996**, *35*, 1154−1196. (e) *Supramolecular Photochemistry*; Balzani, V., Scandola, F., Eds.; Ellis Horwood: Chichester, U.K., 1991.

(2) *Interfacial Supramolecular Assemblies*; Forster, R. J., Keyes, T. E., Vos, J. G., Eds.; Wiley: New York, 2003.

(3) Soi, A.; Hirsch, A. *New J. Chem.* **1999**, *12*, 1337−1339.

(4) *Nanobiotechnology*; Niemeyer, C. M., Mirkin, C. A., Eds.; Wiley-VCH: Weinheim, Germany, 2004.

(5) (a) Whitesides, G. M.; Mathias, J. P.; Seto, C. T. *Science* **1991**, *254*, 1312−1319. (b) Lehn, J. M. *Science* **2002**, *295*, 2400−2403. (c) Whitesides, G. M.; Grzybowski, B. *Science* **2002**, *295*, 2418−2421.

(6) Nuraje, N.; Banerjee, I. A.; MacCuspie, R. I.; Yu, L.; Matsui, H. *J. Am. Chem. Soc.* **2004**, *126*, 8088−8089.

(7) Whitesides, G. M.; Xia, Y. *Angew. Chem., Int. Ed. Engl.* **1998**, *37*, 550−575.

(8) (a) Nuzzo, R. G.; Allara, D. L. *J. Am. Chem. Soc.* **1983**, *105*, 4481−4483. (b) Dubois, L. H.; Nuzzo, R. G. *Annu. Rev. Phys. Chem.* **1992**, *43*, 437−463. (c) Porter, M. D.; Bright, T. B.; Allara, D. L.; Chidsey, C. E. D. *J. Am. Chem. Soc.* **1987**, *109*, 3559−3568.

(9) (a) Love, J. C.; Estroff, L. A.; Kriebel, J. K.; Nuzzo, R. G.; Whitesides, G. M. *Chem. Rev.* **2005**, *105*, 1103−1169. (b) Ulman, A. *Chem. Rev.* **1996**, *96*, 1533−1554.

(10) Enriquez, E. P.; Gray, C. H.; Guarisco, V. F.; Linton, R. V.; Mar, D. K.; Samulski, E. T. *J. Vac. Sci. Technol.* **1992**, *10*, 2775−2782.

(11) *Biochemistry*; Mathews, C. K., Van Holde, K. E., Eds.; Benjamin-Cummings Publ. Co.: San Francisco, CA, 1995.

(12) Long, Y. T.; Irhayem, E. A.; Kraatz, H. B. *Chem. Eur. J.* **2005**, *11*, 5186−5194.

(13) (a) Venanzi, M; Pace, G.; Palleschi, A.; Stella, L.; Castrucci, P.; Scarselli, M.; De Crescenzi, M.; Formaggio, F.; Toniolo, C.; Marletta, G. *Surf. Sci.* **2006**, *600*, 409−416. (b) Pace, G.; Venanzi, M; Castrucci, P.; Scarselli, M.; De Crescenzi, M.; Palleschi, A.; Stella, L.; Formaggio, F.; Toniolo, C.; Marletta, G. *Mater. Sci. Eng., C* **2006**, *26*, 918−923. (c) Gatto, E.; Venanzi, M.; Palleschi, A.; Stella, L.; Pispisa, B.; Lorenzelli, L.; Toniolo, C.; Formaggio, F.; Marletta., G. *Mater. Sci. Eng., C* **2007**, *27*, 1309−1312.

(14) Gatto, E.; Stella, L.; Formaggio, F.; Toniolo, C.; Lorenzelli, L.; Venanzi, M. *J. Pept. Sci.* **2008**, *14*, 184−191.

(15) (a) Gatto, E.; Stella, L.; Baldini, C.; Venanzi, M.; Toniolo, C.; Formaggio, F. *Superlattices Microstruct.* **2009**, *46*, 34−39. (b) Gatto, E.; Caruso, M.; Porchetta, A.; Toniolo, C.; Formaggio, F.; Crisma, M.; Venanzi, M. *J. Pept. Sci.* **2011**, *17*, 124−131.

(16) Wada, A. *Adv. Biophys.* **1976**, *9*, 1−63.

(17) Miura, Y.; Kimura, S.; Kobayashi, S.; Iwamoto, M.; Imanishi, Y.; Umemura, U. *Chem. Phys. Lett.* **1999**, *315*, 1−6.

(18) (a) Galoppini, E.; Fox, M. A. *J. Am. Chem. Soc.* **1996**, *118*, 2299−2300. (b) Galoppini, E.; Fox, M. A. *J. Am. Chem. Soc.* **1997**, *119*, 5277−5285. (c) Shin, J. K.; Newton, M. D.; Isied, S. S. *J. Am. Chem. Soc.* **2003**, *125*, 3722−3732. (d) Umehara, S.; Pourmand, N.; Webb, C. D.; Davis, R. W.; Yasuda, K.; Karhanek, M. *Nano Lett.* **2006**, *6*, 2486−2492. (e) Gatto, E.; Porchetta, A.; Stella, L.; Guryanov, I.; Formaggio, F.; Toniolo, C.; Kaptein, B.; Broxterman, Q. B.; Venanzi, M. *Chem. Biodiversity* **2008**, *5*, 1263−1278.

(19) Sek, S.; Tolak, A.; Misicka, A.; Palys, B.; Bilewicz, R. *J. Phys. Chem. B* **2005**, *109*, 18433−18438.

(20) Yasutomi, S.; Morita, T.; Imanishi, Y.; Kimura, S. *Science* **2004**, *304*, 1944−1947.

(21) (a) Wain, A. J.; Do, H. N. L.; Mandal, H. S.; Kraatz, H. B.; Zhou, F. *J. Phys. Chem. C* **2008**, *112*, 14513−14519. (b) Mandal, H. S.; Kraatz, H. B. *Chem. Phys.* **2006**, *326*, 246−251.

(22) (a) Kimura, S. *Org. Biomol. Chem.* **2008**, *6*, 1143−1148. (b) Niwa, M.; Murata, T.; Kitamastu, M.; Matsumoto, T.; Higashi, N. *J. Mater. Chem.* **1999**, *9*, 343−344.

(23) Balaram, P. *Curr. Opin. Struct. Biol.* **1992**, *2*, 845−851.

(24) Toniolo, C.; Crisma, M.; Formaggio, F.; Peggion, C. *Biopolymers (Pept. Sci.)* **2001**, *60*, 396−419.

(25) Fendler, J. H. *Chem. Mater.* **2001**, *13*, 3196−3210.

(26) Khazraji, A. C.; Hotchandani, S; Das, S.; Kamat, P. V. *J. Phys. Chem. B* **1999**, *103*, 4693−4700.

(27) Kuhn, J. H.; Braslavsky, S. E.; Schmidt, R. *Pure Appl. Chem.* **1989**, *61*, 187−210.

(28) (a) Ozoemena, K.; Nyokong, T. *Electrochim. Acta* **2002**, *47*, 4035−4043. (b) Krysiński, P.; Smolska, M. B. *J. Electroanal. Chem.* **1997**, *424*, 61−67.

(29) Kai, M; Takeda, K.; Morita, T.; Kimura, S. *J. Pept. Sci.* **2008**, *14*, 192−202.
(30) (a) Okamoto, S.; Morita, T.; Kimura, S. *Langmuir* **2009**, *25*, 3297−3307. (b) Takeda, K.; Morita, T.; Kimura, S. *J. Phys. Chem. B* **2008**, *112*, 12840−12850.
(31) *Photophysics of Aromatic Molecules*; Birks, J. B., Ed.; Wiley: New York, 1970.
(32) Nakamura, M.; Saito, N.; Takayama, K.; Kumamoto, S.; Yamana, K. *Chem. Lett.* **2007**, *36*, 602−603.
(33) Yanagisawa, K.; Morita, T.; Kimura, S. *J. Am. Chem. Soc.* **2004**, *126*, 12780−12781.
(34) Morita, T.; Kimura, S.; Kobayashi, S.; Imanishi, Y. *J. Am. Chem. Soc.* **2000**, *122*, 2850−2859.
(35) Yasutomi, S.; Morita, T.; Kimura, S. *J. Am. Chem. Soc.* **2005**, *127*, 14564−14565.
(36) Mandal, H. S.; Burgess, I. J.; Kraatz, H. B. *Chem. Commun.* **2006**, 4802−4804.
(37) (a) Kitagawa, K.; Morita, T.; Kawasaki, M.; Kimura, S. *J. Polym. Sci., Part A: Polym. Chem.* **2003**, *41*, 3493−3500. (b) Kitagawa, K.; Morita, T.; Kimura, S. *Thin Solid Film* **2006**, *509*, 18−26.
(38) Kitagawa, K.; Morita, T.; Kimura, S. *J. Phys. Chem. B* **2004**, *108*, 15090−15095.
(39) Kitagawa, K.; Morita, T.; Kimura, S. *Angew. Chem., Int. Ed.* **2005**, *44*, 6330−6333.
(40) Poirier, G. E. *Chem. Rev.* **1997**, *97*, 1117−1127.
(41) Kim, Y. T.; Bard, A. J. *Langmuir* **1992**, *8*, 1096−1106.
(42) (a) Dubois, L. H.; Zegarski, B. R.; Nuzzo, R. G. *J. Chem. Phys.* **1993**, *98*, 678−688. (b) Poirier, G. E.; Tarlov, M. J.; Rushmeier, H. E. *Langmuir* **1994**, *10*, 3383−3386. (c) Camillone, N.; Eisenberg, P.; Leung, T. Y. B.; Schwartz, P.; Poirier, G. E.; Scoles, G.; Tarlov, M. J. *J. Chem. Phys.* **1994**, *101*, 11031−11034.
(43) (a) Piva, P. G.; Wolkow, R. A.; Kirczenow, G. *Phys. Rev. Lett.* **2008**, *101*, 106801. (b) Battaglini, N.; Klein, H.; Dumas, Ph; Moustrou, C.; Samat, A. *Appl. Surf. Sci.* **2003**, *212*−*213*, 481−484.
(44) (a) Bumm, L. A.; Arnold, J. J.; Charles, L. F.; Dunbar, T. D.; Allara, D. L.; Weiss, P. S. *J. Am. Chem. Soc.* **1999**, *121*, 8017−8021. (b) Pace, G.; Petitjean, A.; Lalloz-Vogel, M. N.; Harrowfield, J.; Lehn, J. M.; Samorì, P. *Angew. Chem.* **2008**, *120*, 2518−2522.
(45) Widrig, C. A.; Chung, C.; Porter, M. D. *J. Electroanal. Chem.* **1991**, *310*, 335−359.
(46) Zhang, J.; Welinder, A. C.; Chi, Q.; Ulstrup, J. *Phys. Chem. Chem. Phys.* **2011**, *13*, 5526−5545.
(47) Walczak, M. M.; Popenoe, D. D.; Deinhammer, R. S.; Lamp, B. D.; Chung, C.; Porter, M. D. *Langmuir* **1991**, *7*, 2687−2693.
(48) Ghaly, T.; Wildt, B. E.; Searson, P. C. *Langmuir* **2010**, *26*, 1420−1423.
(49) Dong, Y.; Abaci, S.; Shannon, C. *Langmuir* **2003**, *19*, 8922−8926.
(50) Howie, J. K.; Houts, J. J.; Sawyer, D. T. *J. Am. Chem. Soc.* **1977**, *99*, 6323−6326.
(51) Konopka, S. J.; McDuffie, B. *Anal. Chem.* **1970**, *42*, 1741−1746.